Current Biology, Volume *31*

Supplemental Information

Narrow mutational signatures drive acquisition of multidrug resistance in the fungal pathogen *Candida glabrata*

Ewa Ksiezopolska, Miquel Àngel Schikora-Tamarit, Reinhard Beyer, Juan Carlos Nunez-Rodriguez, Christoph Schüller, and Toni Gabaldón

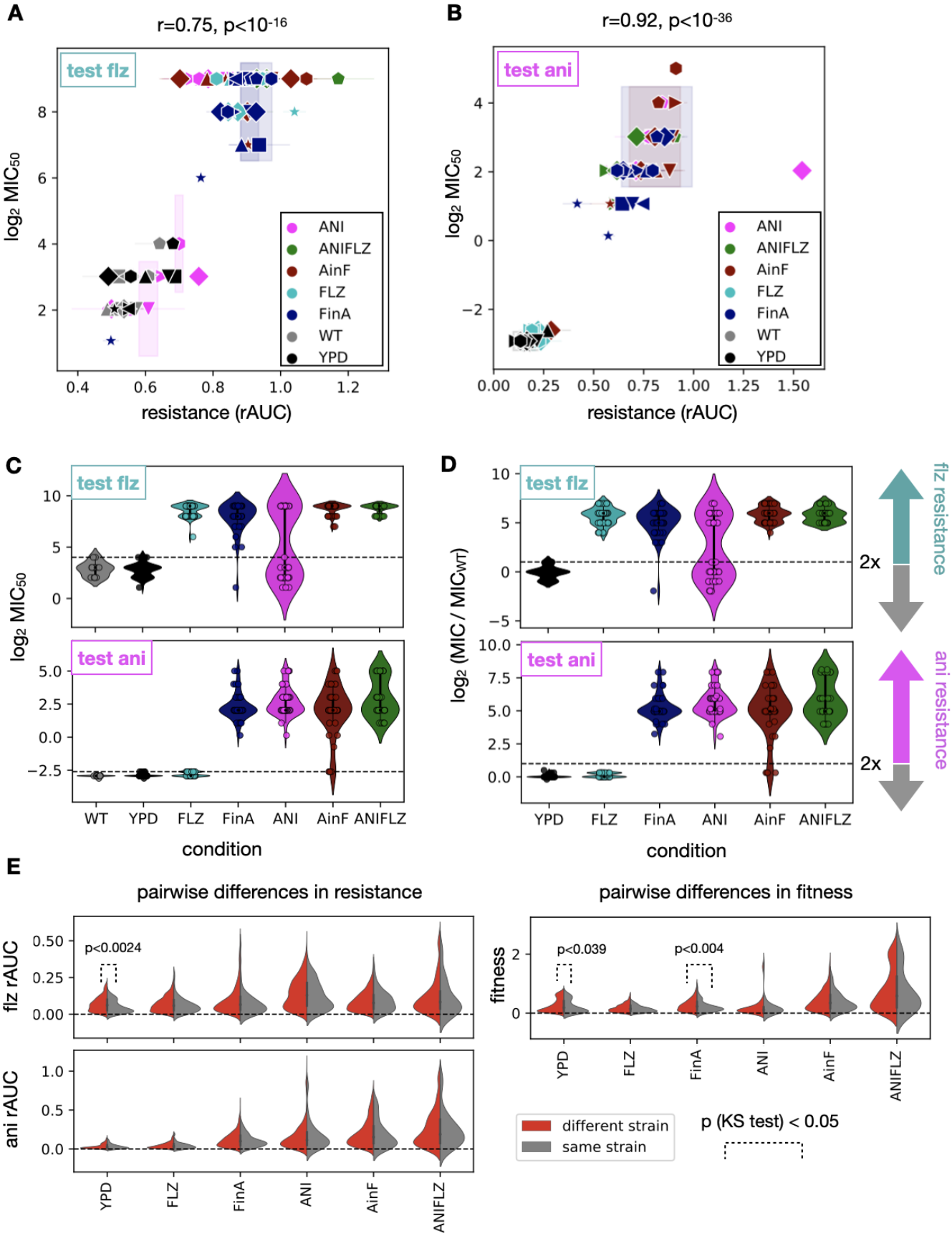
A
r=0.75, p<10-16
test flz
log2 MIC50
resistance (rAUC)
ANI
ANIFLZ
AinF
FLZ
FinA
WT
YPD
B
r=0.92, p<10-36
test ani
log2 MIC50
resistance (rAUC)
C
test flz
test ani
log2 MIC50
WT YPD FLZ FinA ANI AinF ANIFLZ
condition
D
test flz
test ani
log2 (MIC / MICWT)
2x
2x
flz resistance
ani resistance
YPD FLZ FinA ANI AinF ANIFLZ
condition
E
pairwise differences in resistance
flz rAUC
p<0.0024
ani rAUC
YPD FLZ FinA ANI AinF ANIFLZ
pairwise differences in fitness
fitness
p<0.039
p<0.004
YPD FLZ FinA ANI AinF ANIFLZ
different strain
same strain
p (KS test) < 0.05

Figure S1. Comparing Minimum Inhibitory Concentration (MIC) and rAUC. Related to Figure 2.

(A) We compared the flz resistance levels estimated from rAUC and MIC_{50}. The Spearman correlation coefficients and p-values are shown. Each point corresponds to a biological replicate and the error bars reflect the median absolute deviation across technical replicates. **(B)** The same as in (A) but for ani resistance. **(C)** MIC_{50} for flz (top) and ani (bottom) was measured for all samples, presented here as single points. The dashed line indicates the maximum observed value in a YPD sample. **(D)** The increase in MIC relative to WT was calculated as the log2 ratio of MIC of the sample and MIC of WT. Resistant samples are defined as those having a MIC twice as high as the corresponding WT (dashed line). **(E)** Investigating the repeatability of our *in vitro* evolution experiment. We measured the pairwise differences in flz susceptibility (top left), ani susceptibility (bottom left) and fitness (right) between evolved samples of the same (gray) or different (red) strains. The quantitative phenotypes shown in the y axis are similar to **Figure 2B,D**. The x axis shows the evolution condition. In order to test whether the evolution of these phenotypes is particularly repeatable across samples of the same strain we compared the distribution of different-strain (red) vs same-strain (gray) pairwise differences in each condition. This yielded significant differences ($p<0.05$ in a Kolmogorov-Smirnov (KS) test) for some comparisons, indicated with dashed lines.

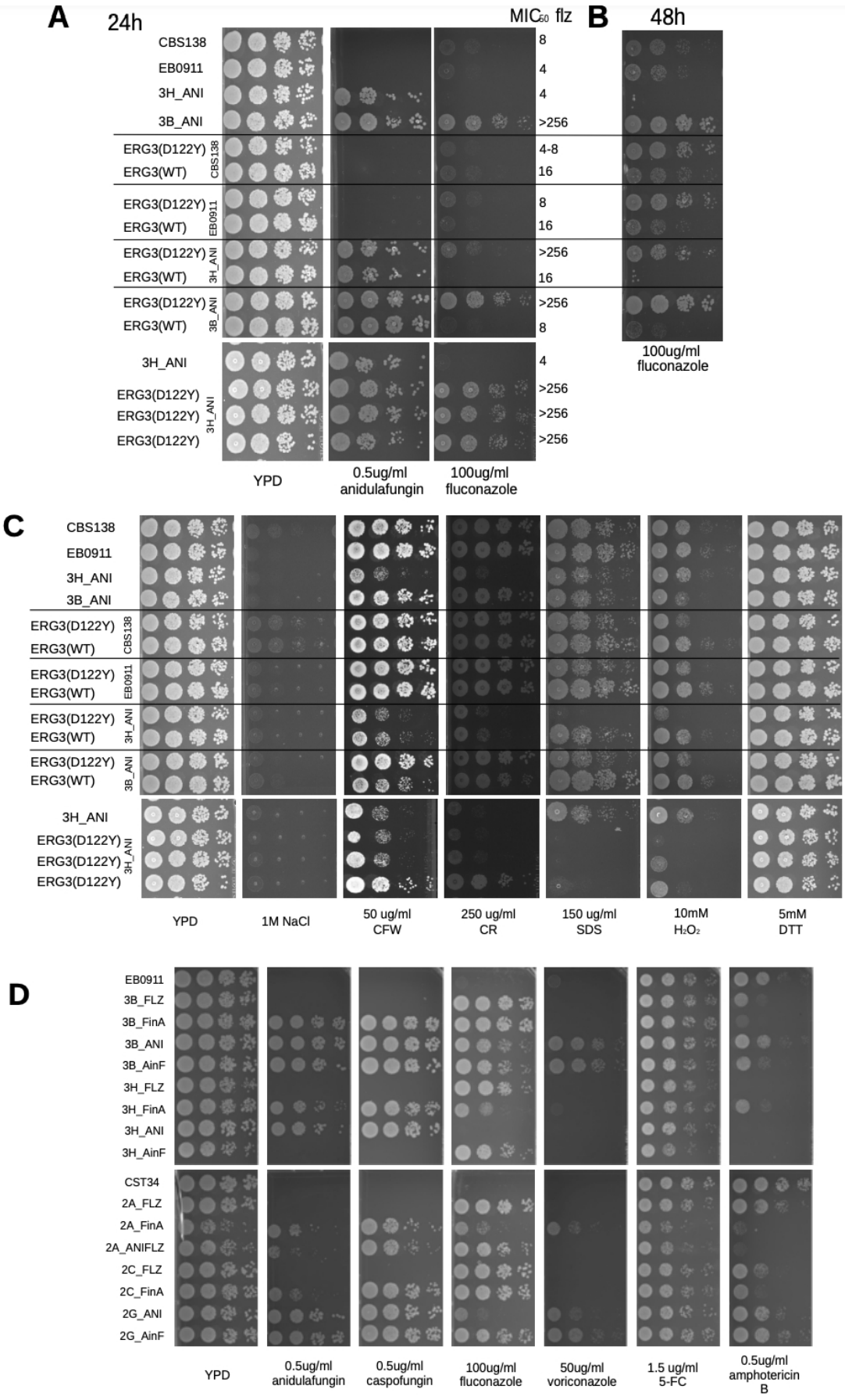
A
24h
MIC50 flz
CBS138
EB0911
3H_ANI
3B_ANI
ERG3(D122Y)
ERG3(WT)
CBS138
EB0911
3H_ANI
3B_ANI
8
4
4
>256
4-8
16
8
16
>256
16
>256
8
4
>256
>256
>256
YPD
0.5ug/ml anidulafungin
100ug/ml fluconazole
B
48h
100ug/ml fluconazole
C
CBS138
EB0911
3H_ANI
3B_ANI
ERG3(D122Y)
ERG3(WT)
YPD
1M NaCl
50 ug/ml CFW
250 ug/ml CR
150 ug/ml SDS
10mM H2O2
5mM DTT
D
EB0911
3B_FLZ
3B_FinA
3B_ANI
3B_AinF
3H_FLZ
3H_FinA
3H_ANI
3H_AinF
CST34
2A_FLZ
2A_FinA
2A_ANIFLZ
2C_FLZ
2C_FinA
2G_ANI
2G_AinF
YPD
0.5ug/ml anidulafungin
0.5ug/ml caspofungin
100ug/ml fluconazole
50ug/ml voriconazole
1.5 ug/ml 5-FC
0.5ug/ml amphotericin B

Figure S2. Spot tests. Related to the samples with re-introduced *ERG3* mutations and susceptibility to a wide panel of drugs and STAR Methods.

(**A**) Susceptibility of transformants carrying introduced changes in *ERG3* gene. Spot tests demonstrate changes in susceptibility (on a rich medium YPD supplemented with 100ug/ml flz and 0.5ug/ml ani) followed by EUCAST test after 24h incubation. The first four strains are the background strains used for the transformation: wild type *Candida glabrata* CBS138 and EB0911 as well as ani evolved progenies of EB0911: 3H_ANI (susceptible to flz) and 3B_ANI (bearing *ERG3* D122Y mutation and resistant to flz). The following spots represent the susceptibility of transformants carrying: *ERG3*(WT) or *ERG3*(D122Y) alleles fused with a *NAT1* selection marker. The bottom panel shows three independent transformants carrying *ERG3*(D122Y) mutation inserted into an ani resistant strain (3H_ANI) - 1. transformed with a long fragment with *ERG3* and crRNA_ERG3_1 and 2. and 3. are 2 different colonies obtained from a transformation with synthetic *ERG3* fragment and crRNA_ERG3_2. These transformants do not contain *NAT1* gene and were selected on flz. Note that **Table S5** includes the list of used oligos. (**B**) presents a spot test of CRISPR transformants grown on flz and incubated for 48h. (**C**) shows susceptibility of *ERG3* CRISPR transformants to NaCl, Calcofluor White (CFW), Congo Red (CR), SDS, H_20_2 and DTT. (**D**) presents susceptibility of selected evolved mutants to anidulafungin, caspofungin, fluconazole, voriconazole, flucytosine (5-FC) and amphotericin B. Used concentrations are indicated in the figure.

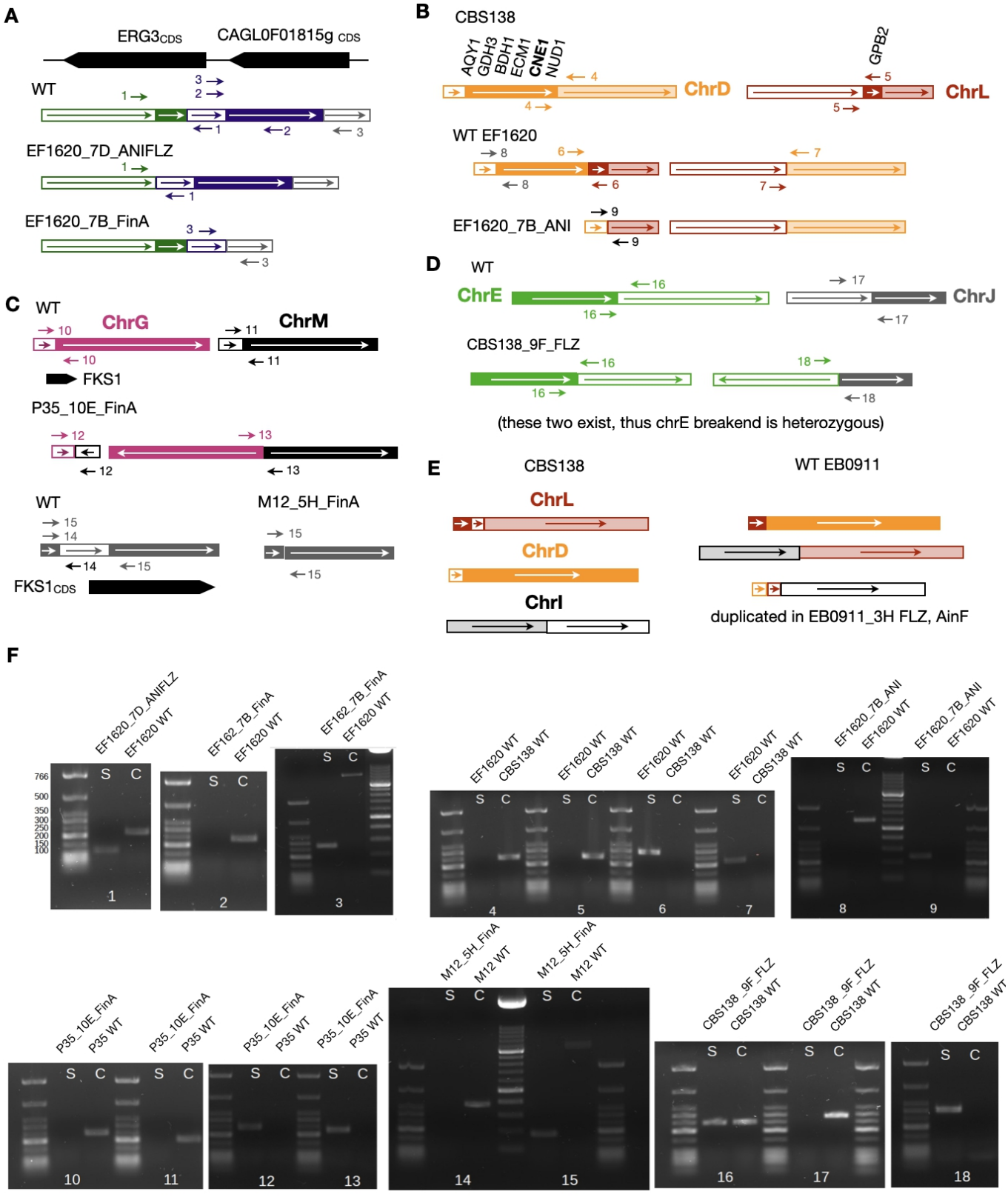

Figure S3. Genomic rearrangements that appear during evolution in antifungal drugs. Related to Figure 6.

(A) We found two samples with a deletion in the *ERG3* CDS (medium) and upstream region (bottom), respectively. The browser represents the genomic coordinates of *ERG3* and the upstream gene *CAGL0F01815g*. The boxes represent the WT regions that are rearranged in each sample. We confirmed these rearrangements with three PCRs on these samples (using primer pairs 1, 2 and 3). The results are

shown in (F), with the numbers matching the primer pairs of each PCR. **(B)** *CNE1* and *GBP2* were lost due to a single deletion rearrangement in EF1620_7B_ANI. The representation is analogous to (A), showing a EF1620 WT balanced translocation between Chr D and L which, in addition to the deletion-like breakpoint appearing in ANI, generates a loss of the region between the two breakpoints. **(C)** Two FinA samples carried rearrangements breaking the *FKS1* CDS (black box). P35_10E_FinA had an inverted balanced translocation between Chrs G and J (top), and M12_5H_FinA carried a partial deletion (bottom). **(D)** Genomic rearrangements can explain the partial Chr E aneuploidy in CBS138_9F_FLZ **(Figure 5A)**. This sample carried an unbalanced translocation between Chr E and J. Both Chr E breakends were heterozygous, while the Chr J breakend was haploid. **(E)** The apparent partial duplication of Chr I **(Figure 5A)** is actually a complete aneuploidy in two EB0911 samples. We found WT balanced translocations between these chromosomes that result in three mixed chromosomes in this strain (bottom). We found that two EB0911_3H samples had one of these mixed chromosomes duplicated (bottom), including mostly half of the reference Chr I. **(F)** We performed PCRs using primer pairs around the rearrangements (1 to 18 in **(A)** - **(D)**) to confirm them. These primers can be found in **Table S5.** Each PCR was carried on a given sample and the corresponding control. We note that we could obtain bands with the expected sizes in all samples.

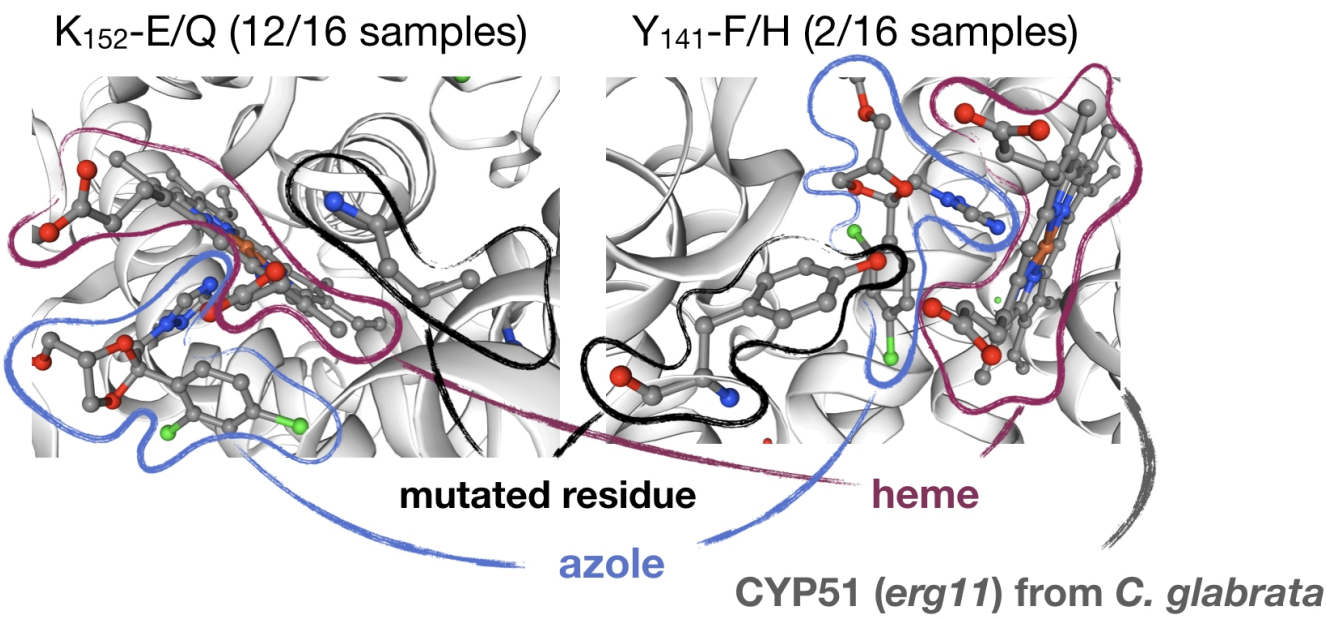

Figure S4. Structural localization of frequent *ERG11* mutations. Related to Figure 6.

Given the availability of a characterized 3D structure for Erg11p in contact with azoles (pdb id: 5JLC) we inspected the location of recurrently mutated residues and found that they are close to the azole binding pocket. The structure (pdb id: 5JLC) was visualized using SWISS MODEL[S1]. A screenshot of the two residues in the context of itraconazole and a heme group is shown. The basic group of K152 is close to an acid group in heme, potentially establishing an electrostatic interaction that is important for stability. Importantly, Y141 is conserved with Y132, a position that has been mutated in various other azole resistant *Candida* species[S2-S4]. As a possible mechanism of resistance, we hypothesize that the substitution by E or Q destabilizes this interaction, thereby impairing the binding of azoles.

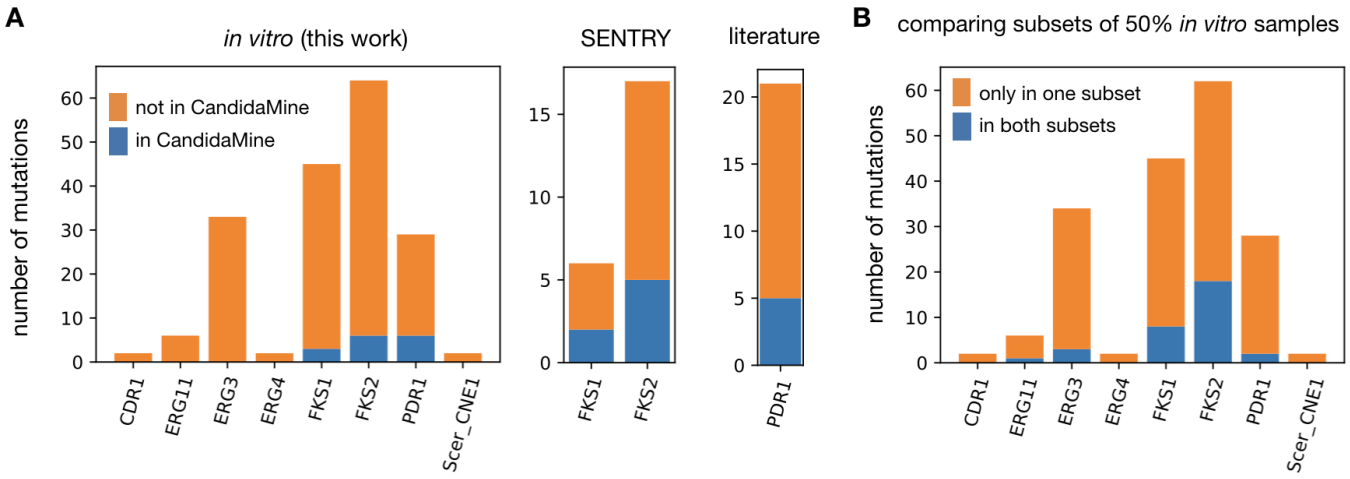

Figure S5. The overlap between drug resistance-conferring mutations from different studies in *Candida glabrata*. Related to the analysis of clinical isolates' sequencing datasets in STAR Methods.

(A) We compared the drug resistance variants described in this work (left), the SENTRY database (middle[S5]) and a set of described *PDR1* mutations (right[S6-S8]) against those in clinical isolates with available whole genomes (393 in total) (see **STAR Methods**). Shown is the number of mutations that are found in each study and in some (blue) or no (orange) clinical isolates. **(B)** In order to estimate the expected overlap between drug resistance mutations among different samples, we implemented a randomised strategy from our own experiments. We divided the samples carrying mutations in a given gene into two random subsets. For each subset, we calculated the number of mutations only in the subset or also found in the other subset. This process was repeated 100 times, and shown is the median number of mutations not shared (orange) or shared (blue) across subsets.

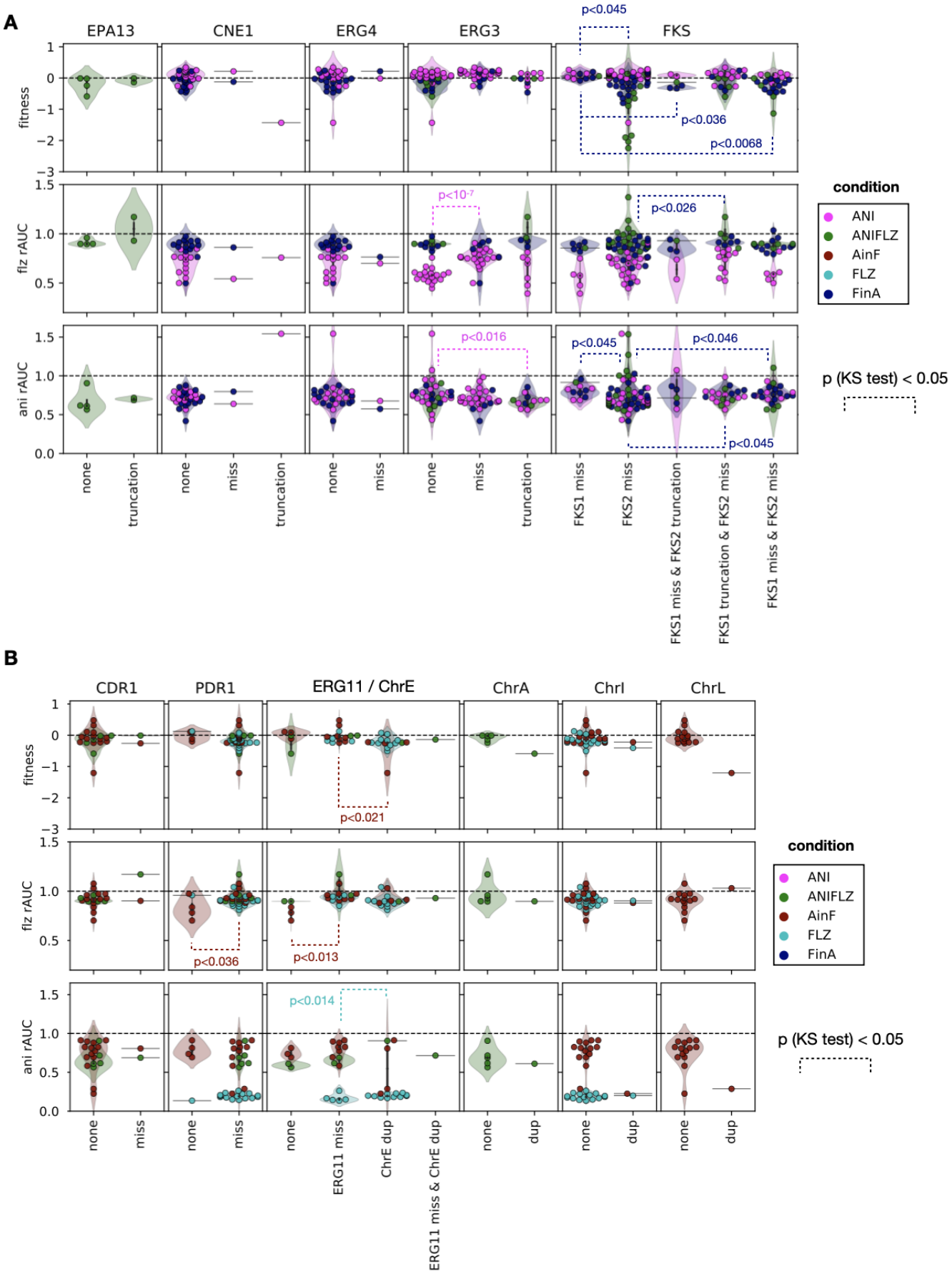
A
EPA13
CNE1
ERG4
ERG3
FKS
p<0.045
p<0.036
p<0.0068
fitness
flz rAUC
ani rAUC
p<10-7
p<0.026
p<0.016
p<0.045
p<0.046
p<0.045
condition
ANI
ANIFLZ
AinF
FLZ
FinA
p (KS test) < 0.05
none
truncation
none
miss
truncation
none
miss
none
miss
truncation
FKS1 miss
FKS2 miss
FKS1 miss & FKS2 truncation
FKS1 truncation & FKS2 miss
FKS1 miss & FKS2 miss
B
CDR1
PDR1
ERG11 / ChrE
ChrA
ChrI
ChrL
p<0.021
p<0.036
p<0.013
p<0.014
fitness
flz rAUC
ani rAUC
condition
ANI
ANIFLZ
AinF
FLZ
FinA
p (KS test) < 0.05
none
miss
none
miss
none
ERG11 miss
ChrE dup
ERG11 miss & ChrE dup
none
dup
none
dup
none
dup

Figure S6. Genotype-phenotype relationship in the evolved samples. Related to Figures 2 and 6.

(A) Similar mutations in genes altered during evolution in ani seldom modulate fitness (top), flz susceptibility (medium) or ani susceptibility (bottom). The y axis shows each quantitative phenotype as in **Figure 2B,D**. Each point represents one *in vitro*-evolved sample and the color indicates the condition. The x axis shows whether each sample has no mutations ("none"), missense mutations ("miss") or truncating mutations ("truncation") in the given gene. In addition, we separate the samples by *FKS1/FKS2* mutation status (right panel) in order to show how different combinations of mutations in these genes may affect each phenotype. We compared the phenotypes for each of the condition/mutation type combinations in a pairwise manner with a Kolmogorov-Smirnov (KS) test to find significant differences between the groups. The dashed lines correspond to comparisons with a $p<0.05$. **(B)** The same as in (A), but for genes / chromosomes mutated during evolution in flz. The "ERG11 / ChrE" panels shows these phenotypes for different combinations of *ERG11* missense mutations and Chr E duplications ("ChrE dup"). The samples in the rightmost three panels are separated by the absence ("none") or presence ("dup") of chromosomal duplications.

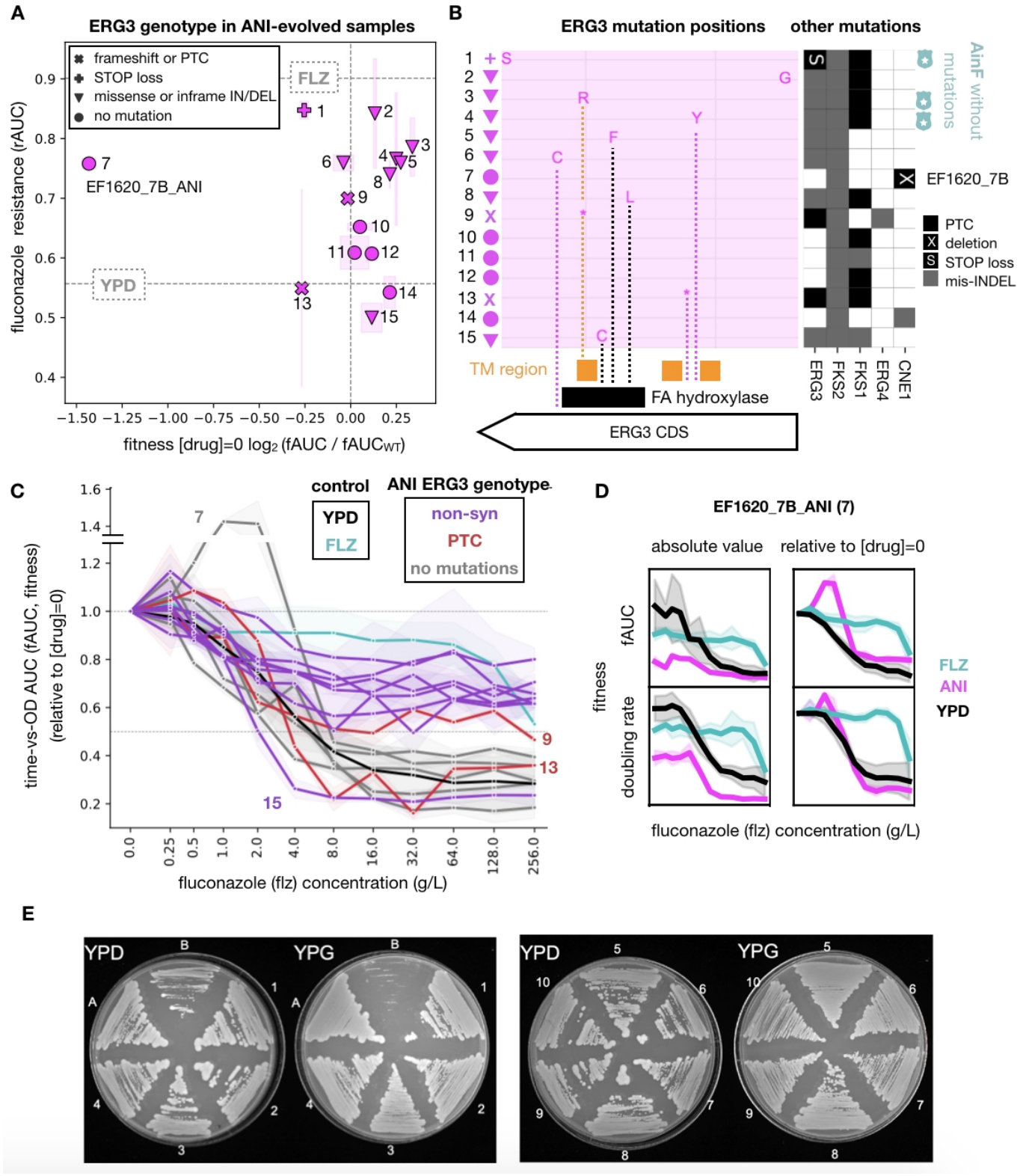

Figure S7. Acquisition of *ERG3* mutations in ANI samples and fluconazole cross-resistance. Related to Figure 7.

(A) Fitness (relative to the WT as in **Figure 2D**) is high in most ANI-evolved samples (EF1620_7B_ANI is an exception), while flz-resistance (shown as rAUC) is variable. The symbols correspond to different types of *ERG3* protein-altering mutations. The dashed lines correspond to the median flz rAUC for all the FLZ and YPD samples. Each point represents the median across technical replicates for a given sample, while the boxes show the median absolute deviation. The numbers are related to the order of flz-

resistance used to show the relationship of each sample to panels (B), (C) and (D). **(B)** *ERG3* amino acid mutations are scattered throughout the coding region of the gene. The boxes in the bottom represent annotated protein domains (see **STAR Methods**), where the "catalytic domain" is the Fatty acid (FA) hydroxylase superfamily (PF04116) and TM are transmembrane regions. Three samples with no additional mutations nor increase in flz resistance in subsequent flz treatment (AinF) are marked with blue shields. PTC and '*' indicate Premature Termination and S indicates the loss of the STOP codon. **(C)** Growth of the ANI samples (with colored *ERG3* genotype) at increasing concentrations of flz shown as fAUC and compared to all FLZ (blue) and YPD (black) samples. Purple lines indicate samples with non-synonymous alterations, red - with protein termination codon (PTC) and gray - no *ERG3* changes. Samples 9 and 13 bear a PTC but the former showed improved growth at higher flz concentrations. Although assessed as susceptible based on MIC, sample 9 presented a growth curve more similar to that of resistant samples, and maintained a relative growth around ~50% across increasing concentrations (see **Analysis of MIC and rAUC measures for antifungal drug resistance in STAR methods**). Sample 15 bears the only ns mutation that did not result in increased resistance to flz by rAUC, MIC or shape and position of the growth curve. The points and error bars correspond to the median and median absolute deviation for each assayed concentration in each sample, respectively. The numbers (7, 15, 9, 13) correspond to those in (A) and (B). **(D)** EF1620_7B_ANI (number 7 in this figure) was found to be susceptible to flz according to our MIC-based thresholding (**Figure S1C,D**) but depicted an rAUC in the range of resistant samples (A). To understand this mismatch, we studied the quantitative relationship between flz concentration and several fitness estimates (the doubling rate per hour (bottom) and fAUC (top)) in both absolute (left) and relative to no drug (right) representations. The median values across all FLZ and YPD EF1620 samples are shown for comparison. **(E)** Petite phenotype assessment. Growth of ANI evolved mutants (1. 2G_ANI, 2. 3B_ANI, 3. 5F_ANI, 4. 7D_ANI, 5.7F_ANI, 6. 9F_ANI, 7. 9H_ANI, 8. 10G_ANI, 9. 11G_ANI, 10. 11H_ANI), CBS138 (A) and petite *S. cerevisiae* mutant (B), on YP medium supplemented with glucose (YPD) and glycerol (YPG).

Systematic name	Standard name or ortholog	CST109	M12	description
CAGL0C05313g	-	N547H	M206V	Protein of unknown function
CAGL0B01166g	SWI6	A246T	R414K	Ortholog(s) have DNA-binding transcription activator activity, RNA polymerase II-specific, RNA polymerase II proximal promoter sequence-specific DNA binding, transcription coactivator activity
CAGL0E03564g	Scer_CDC3	K383R	I278M	Ortholog(s) have GTP binding, phosphatidylinositol-4-phosphate binding, phosphatidylinositol-5-phosphate binding, structural molecule activity
CAGL0G01430g	Scer_LAP2	N469S	P222S	Ortholog(s) have aminopeptidase activity, epoxide hydrolase activity and role in cellular lipid metabolic process, protein catabolic process, protein localization by the NVT pathway
CAGL0H03179g	**Scer_MAD1**	**Y390H**	**D387N**	**Ortholog(s) have protein-containing complex binding activity**
CAGL0H09130g	Scer_MNN4	R573Stop	P734A	Ortholog(s) have enzyme activator activity and role in fungal-type cell wall polysaccharide biosynthetic process, protein N-linked glycosylation, protein O-linked glycosylation
CAGL0H02255g	Scer_RSN1	E709G	I787M	Ortholog(s) have role in Golgi to plasma membrane transport and membrane localization
CAGL0J07326g	Scer_SQS1	Q359L	D533E	Ortholog(s) have role in mRNA splicing, via spliceosome, maturation of SSU-rRNA, positive regulation of ATPase activity, positive regulation of helicase activity

Table S1. List of shared polymorphisms found in CST109 (clade 1) and M12 (clade 3) that were not found in other representatives of their respective clades - CST34 and CST78 for clade 1 and 3, respectively. Related to the Results section '*Candida glabrata* has a widespread ability to acquire drug and multidrug resistance' and STAR Methods.

We highlight the ortholog of *Saccharomyces cerevisiae MAD1* for which polymorphisms in CST109 and M12 were found to affect nearby residues in the protein sequence (390 and 387, respectively). Dysfunction of this gene has been previously related to chromosome instability in *S. cerevisiae*[S9]. Thus, these polymorphisms might be associated with higher chromosome instability resulting in lower capacity to preserve long-term drug resistance.

					genome sequencing	sanger sequencing
Mutant	**Condition**	**Clade**	**Strain**	**Replicate**	***ERG3***	
TGL00051	ANI	1	CST109	1B		-
TGL00052	ANI	1	CST109	1D		-
TGL00053	ANI	1	CST109	1F		-
TGL00054	ANI	1	CST109	1H		-
TGL00055	ANI	1	CST34	2A	-	
TGL00056	ANI	1	CST34	2C		mis|p.213|L/S
TGL00057	ANI	1	CST34	2E		ins|c.215|TC, ins|p.77|
TGL00058	ANI	1	CST34	2G	mis|p.207|P/L	
TGL00059	ANI	2	EB0911	3B	mis|p.122|D/Y	
TGL00060	ANI	2	EB0911	3D		-
TGL00061	ANI	2	EB0911	3F		-
TGL00062	ANI	2	EB0911	3H	-	
TGL00063	ANI	3	CST78	4A		-
TGL00065	ANI	3	CST78	4E		mis|p.1|M/L
TGL00066	ANI	3	CST78	4G		PTC|p.67|Y/*
TGL00067	ANI	3	M12	5B		-
TGL00068	ANI	3	M12	5D		mis|p.265|N/K
TGL00069	ANI	3	M12	5F	mis|p.9|D/G	-
TGL00070	ANI	3	M12	5H	-	
TGL00071	ANI	4	EF1237	6A		-
TGL00072	ANI	4	EF1237	6C		mis|p.302|Q/K
TGL00073	ANI	4	EF1237	6E		-
TGL00074	ANI	4	EF1237	6G		-
TGL00075	ANI	4	EF1620	7B	-	
TGL00076	ANI	4	EF1620	7D	mis|p.267|W/R	
TGL00077	ANI	4	EF1620	7F	mis|p.243|Y/C	
TGL00078	ANI	4	EF1620	7H		-
TGL00079	ANI	5	F15	8A		-
TGL00080	ANI	5	F15	8C		mis|p.224|T/A
TGL00081	ANI	5	F15	8E		-
TGL00082	ANI	5	F15	8G		mis|p.135|Q/R
TGL00083	ANI	5	CBS138	9B		mis|p.128|H/Y
TGL00084	ANI	5	CBS138	9D		partial deletion
TGL00085	ANI	5	CBS138	9F	PTC|p.135|Q/*	
TGL00086	ANI	5	CBS138	9H	STOP|c.1094|tAg/tCg	
TGL00087	ANI	6	P352	10A		PTC|p.239|Q/*
TGL00088	ANI	6	P352	10C		mis|p.71|P/L
TGL00089	ANI	6	P352	10E	-	
TGL00090	ANI	6	P352	10G	mis|p.228|S/F	
TGL00091	ANI	7	BG2	11B	mis|p.300|Y/C	
TGL00092	ANI	7	BG2	11D		mis|p.87|R/I
TGL00093	ANI	7	BG2	11F		mis|p.300|Y/C
TGL00094	ANI	7	BG2	11H	PTC|p.267|W/*	
TGL00096	ANI	7	SLL2glab	12A		mis|p.225|P/T
TGL00095	ANI	7	SLL2glab	12C		mis|p.301|G/D
TGL00097	ANI	7	SLL2glab	12E		mis|p.225|P/T
TGL00098	ANI	7	SLL2glab	12G		PTC|p.203|W/*

Table S2. *ERG3* mutations. Related to Figure 7.

Columns indicate, in this order: mutant name, evolution media, clade, strain, replicate, mutations in *ERG3* gene from genome and sanger sequencing. The variants are encoded as “type of mutation” / “molecule affected” . “position” | “reference allele” / “alternative allele”. The “type of mutation” can be: mis - missense variant, del - inframe deletion, PTC – Premature Termination Codon, FS - frameshift, ins – inframe insertion, lostSTOP – lost STOP codon, lostATG - lost START codon. The “molecule affected” can be “p” for protein and “c” for cDNA. The “reference” and “alternative” alleles correspond to amino acids or codons for proteins or cDNA alterations, respectively.

evolution media	ANI			ANI			ANI		ANI			ANI			ANI			ANI			ANI			ANI			ANI		
clade	1			2			3		4			4			5			5			6			4			7		
strain	CST34			EB0911			M12		EF1620			EF1620			CBS138			CBS138			P352			BG2			BG2		
replicate	2G			3B			5F		7D			7F			9F			9H			10G			11B			11H		
tested gene/fragment	FKS2 HS1	ERG3		FKS1 HS1	FKS2 HS1	ERG3	FKS2 HS1	ERG3	FKS1 HS1	FKS2 HS1	ERG3	FKS1 HS1	FKS2 HS1	ERG3	FKS1 HS1	FKS2 HS1	ERG3	FKS2 HS1		ERG3	FKS2 HS1		ERG3	FKS2 HS1		ERG3	FKS2 HS2	ERG3	
final mutation	F659-	P207L	E139*	S652*	F659-	D122Y	F659-	D9G	W650*	F659-	W267R	D632Y	F659L	Y243C	W611*	L662W	Q135*	F659-	F659L	lost STOP	F659-	R665G	S228F	A651V	S663P	Y300C	R1378H	W267*	G301V
			new!																new!										new!
ani (ug/ml)																													
0.032	--			--	--		--		--	--		--	--		--	--		--	--		--	--		A651V	--	--	--		
0.064	--			--	--		--		--	--	--	--	--	--	--	L662W		--	--		--	--		--	--		--		
0.126	--	--	E139*	--	--	--	--	--	--	F659-	W267R	--	F659L	Y243C	--	L662W		--	--	lost STOP	--	--	S228F	A651V	--		--		
0.256	F659-	P207L	--	--	F659-	D122Y	F659-	D9G	--	F659-		--	F659L		--	L662W	--	--	F659L	lost STOP	--	R665G	S228F	A651V	--		--	--	G301V

Table S3. Trajectory of final *FKS* and *ERG3* mutations. Related to Figure 7.

Rows indicate, in this order: evolution media, clade, strain, replicate, tested gene/fragment, final mutation, and concentrations of anidulafungin (μg/ml) corresponding to intermediate glycerol stocks (isolated single colonies) of tested trajectories. Mutations that were not found at the finalization of the evolution experiment are marked as 'new'.

passages	drug increase	fluconazole (μg/mL)	anidulafungin (μg/mL)
		0	0
		0	0
1		4	0.016
2	1	4	0.016
3		8	0.032
4	2	8	0.032
5		16	0.064
6	3	16	0.064
7		32	0.128
8	4	32	0.128
9		64	0.256
10	5	64	0.256
11		96	0.512
12	6	96	0.512
13		128	1.024
14	7	128	1.024
15		160	2.048
16	8	160	2.048
17		192	4.096
18	9	192	4.096

Table S4. Information on drugs' concentrations used in the evolution experiments. Related to Figure 1.

Columns indicate, in this order: number of passages, number of drug increases and corresponding fluconazole and anidulafungin concentrations (μg/mL).

	name	sequence
genome rearrangements	ChrF_1_F	GTAGGACAAAGAGGCGGTGA
	ChrF_1_R	TCTACGCTGCTGCATGAGAC
	ChrF_2_F	CCCAGACAATGGGATGAAAT
	ChrF_2_del_R	TATCATGTGACAGCGTCTGC
	ChrF_3_R	GTGTTGGGCAAAGGTGACTT
	ChrD_1_F	CACCAAAGGAAAGGACAAGG
	ChrD_1_R	CCCTGTTGGTGGTCATTTTT
	ChrL_1_F	TCGCATATGCATTTCATCGT
	ChrL_1_R	AACTGCCTCCAACACTTTCG
	ChrDL_1_F	CAGGTCAAATACGTTTCCCATAA
	ChrDL_1_del_R	TTTCATTTGTTATTGAATATCTTTGC
	ChrDL_2_R	CCAGCAGGAACTCTATCAAGG
	ChrG_1_F	GAAGGTATCGCTAAGATTGTCTTC
	ChrG_1_R	GACCAATTGTTGATAGTTGTGTG
	ChrM_1_F	TTGCGATAGAAGCTTTCCTACA
	ChrM_1_R	TCCGATGTGCCATCAATCTA
	revChrG_1_F	CCAATTGTTGATAGTTGTGTGTG
	revChrM_1_R	TCGATGAGTCCATGAAAAGAAA
	ChrG_2_F	AAGAGGTGAGGGAGGGAGAA
	ChrG_2_del_R	GGGACTAAGCTGATACACGAAGA
	ChrG_3_R	GGCTTGACCATTCTGTTGGT
	ChrE_1_F	TCTGCACCACGGTAGAAAG
	ChrE_1_R	GATGATTGCAAGGAAGAAGAA
	ChrJ_1_F	CTGAATAAGGGTTGCGTGCT
	ChrJ_1_R	ATGAGGGCCCCTGTCTTTAC
	revChrE_1_F	ATGAGGGCCCCTGTCTTTAC
ERG3	ERG3_1_FWD	TTGCATTTCAGATAACCTACAGC
	ERG3_1_REV	CAGTGCAGCCATCTGTGAG
	ERG3_2_FWD	TCCCTCTTGACTGTCCCTTG
	ERG3_2_REV	AAAGTAATGTGTGCGCGAGA
FKS	FKS1_HS1_FWD	CCATTGGGTGGTCTGTTCACG
	FKS1_HS1_REV	GATTGGGCAAAGAAAGAAATACGAC
	FKS1_HS2_FWD	GGTATTTCAAAGGCTCAAAAGGG
	FKS1_HS2_REV	ATGGAGAGAACAGCAGGGCG
	FKS2_HS1_FWD	GTGCTCAACATTTATCTCGTAGG
	FKS2_HS1_REV	CAGAATAGTGTGGAGTCAAGACG
	FKS2_HS2_FWD	CGTAGACCGTTTCTTGACTTC
	FKS2_HS2_REV	CTTGCCAATGTGCCACTG

CRISPR		
ERG3	crRNA_ERG3_1	/AltR1/rGrA rArArA rCrGrU rArGrG rArCrA rArArG rArGrG rGrUrU rUrUrA rGrArG rCrUrA rUrGrC rU/AltR2/
	crRNA_ERG3_2	/AltR1/rUrC rUrGrU rCrGrA rArGrA rCrGrA rArArA rCrGrU rGrUrU rUrUrA rGrArG rCrUrA rUrGrC rU/AltR2/
	donor_ERG3	/Alt-R-HDR1/T*G* GTT CTT CAA GTA TTT TGG ATG GTT GAA GAT AGT TCT GTA GAA GAC GAA AAC GTA TGA CAA AGA GGC GGT GAT CAG GTA CAA TAG CAG ACC GAA GA*C* G/Alt-R-HDR2/
LongFragmentERG3	FL1_FWD	TCCTCGACCAACAGACCATC
	FL1_REV	TGTTCGAGACTAGTAGCGGG
1. FLKI_ERG3	1_flank_ERG3_FWD	TCCTCGACCAACAGACCATC
	1_REV	gtcgacctgcagcgtacgAATGAGAACCCAGGTCAGCAC
2. NAT1(for DNA donor constructs)	2_NAT1_FWD	GTGCTGACCTGGGTTCTCATTcgtacgctgcaggtcgac
	2_NAT1_REV	TTAATTTGTTGCCATAAAAAATctacgagaccgacaccg
3. FLKII	3_FLKII_FWD	cggtgtcggtctcgtagATTTTTTATGGCAACAAATTAA
	3_FLKII_REV	TGTACTGGCACTTCGACCTT
check the fusion	inside_ERG3_FWD	TCCCTCTTGACTGTCCCTTG
	inside_NAT1_REV	caaccacaaatgaccagcac
	inside_NAT1_FWD	gtgatttggctggtttcgtt
	flank_ERG3_REV	GTGGAGGCGAGGAGTAGAAA
after the transformation – in the correct place	out_REV	GGTAGTCAGCAAGGTCTCGT
	inside_NAT1_FWD	gtgatttggctggtttcgtt
double check if NAT inside, primers down and upstream of the *NAT1*	inside_ERG3_FWD	TCCCTCTTGACTGTCCCTTG
	flank_ERG3_REV	GTGGAGGCGAGGAGTAGAAA

Table S5. Information about all the oligos used in the study. Related to Figures: 3, 7, S2, S3 and STAR Methods.

The table includes primers used to confirm the GR, investigate *ERG3* gene and *FKS1* and *FKS2* fragments as well as crRNAs, ordered *ERG3* fragment and primers used in CRISPR-Cas9 transformations. Lowercase letters in primers used in CRISPR Cas9 transformations indicate the sequences in *NAT1* gene.

Supplemental References

S1. Waterhouse, A., Bertoni, M., Bienert, S., Studer, G., Tauriello, G., Gumienny, R., Heer, F.T., de Beer, T.A.P., Rempfer, C., Bordoli, L., et al. (2018). SWISS-MODEL: homology modelling of protein structures and complexes. Nucleic Acids Res. *46*, W296–W303.

S2. Lockhart, S.R., Etienne, K.A., Vallabhaneni, S., Farooqi, J., Chowdhary, A., Govender, N.P., Colombo, A.L., Calvo, B., Cuomo, C.A., Desjardins, C.A., et al. (2017). Simultaneous Emergence of Multidrug-Resistant Candida auris on 3 Continents Confirmed by Whole-Genome Sequencing and Epidemiological Analyses. Clin. Infect. Dis. *64*, 134–140.

S3. Berkow, E.L., Manigaba, K., Parker, J.E., Barker, K.S., Kelly, S.L., and Rogers, P.D. (2015). Multidrug Transporters and Alterations in Sterol Biosynthesis Contribute to Azole Antifungal Resistance in Candida parapsilosis. Antimicrob. Agents Chemother. *59*, 5942–5950.

S4. Tan, J., Zhang, J., Chen, W., Sun, Y., Wan, Z., Li, R., and Liu, W. (2015). The A395T mutation in ERG11 gene confers fluconazole resistance in Candida tropicalis causing candidemia. Mycopathologia *179*, 213–218.

S5. Pfaller, M.A., Diekema, D.J., Turnidge, J.D., Castanheira, M., and Jones, R.N. (2019). Twenty Years of the SENTRY Antifungal Surveillance Program: Results for Candida Species From 1997–2016. Open Forum Infectious Diseases *6*, S79–S94.

S6. Ferrari, S., Ischer, F., Calabrese, D., Posteraro, B., Sanguinetti, M., Fadda, G., Rohde, B., Bauser, C., Bader, O., and Sanglard, D. (2009). Gain of function mutations in CgPDR1 of Candida glabrata not only mediate antifungal resistance but also enhance virulence. PLoS Pathog. *5*, e1000268.

S7. Tsai, H.-F., Sammons, L.R., Zhang, X., Suffis, S.D., Su, Q., Myers, T.G., Marr, K.A., and Bennett, J.E. (2010). Microarray and molecular analyses of the azole resistance mechanism in Candida glabrata oropharyngeal isolates. Antimicrob. Agents Chemother. *54*, 3308–3317.

S8. Spettel, K., Barousch, W., Makristathis, A., Zeller, I., Nehr, M., Selitsch, B., Lackner, M., Rath, P.-M., Steinmann, J., and Willinger, B. (2019). Analysis of antifungal resistance genes in Candida albicans and Candida glabrata using next generation sequencing. PLoS One *14*, e0210397.

S9. Zhu, J., Pavelka, N., Bradford, W.D., Rancati, G., and Li, R. (2012). Karyotypic determinants of chromosome instability in aneuploid budding yeast. PLoS Genet. *8*, e1002719.

S10. Skrzypek, M.S., Binkley, J., Binkley, G., Miyasato, S.R., Simison, M., and Sherlock, G. (2017). The Candida Genome Database (CGD): incorporation of Assembly 22, systematic identifiers and visualization of high throughput sequencing data. Nucleic Acids Res. 45, D592–D596.